

# Probing the dynamics of nanoparticle growth in a flame using synchrotron radiation

GREGORY BEAUCAGE<sup>1\*</sup>, HENDRIK K. KAMMLER<sup>2</sup>, ROGER MUELLER<sup>2</sup>, RETO STROBEL<sup>2</sup>, NIKHIL AGASHE<sup>1</sup>, SOTIRIS E. PRATSINIS<sup>2</sup> AND THEYENCHERI NARAYANAN<sup>3</sup>

<sup>1</sup>Chemical and Materials Engineering, University of Cincinnati, Cincinnati, Ohio 45221-0012, USA

<sup>2</sup>Institut für Verfahrenstechnik, ETH Zentrum ML F26 CH-8092 Zürich, Switzerland

<sup>3</sup>ESRF, F-38043 Grenoble, France

\*e-mail: beaucag@uc.edu

Published online: 16 May 2004; doi:10.1038/nmat1135

**F**lame synthesis is one of the most versatile and promising technologies for large-scale production of nanoscale materials<sup>1–3</sup>. Pyrolysis has recently been shown to be a useful route for the production of single-walled nanotubes<sup>4</sup>, quantum dots<sup>5</sup> and a wide variety of nanostructured ceramic oxides for catalysis<sup>6</sup> and electrochemical applications<sup>7</sup>. An understanding of the mechanisms of nanostructural growth in flames has been hampered by a lack of direct observations of particle growth<sup>8–21</sup>, owing to high temperatures (2,000 K), rapid kinetics (submillisecond scale), dilute growth conditions (10<sup>–6</sup> volume fraction) and optical emission of synthetic flames. Here we report the first successful *in situ* study of nanoparticle growth in a flame using synchrotron X-ray scattering. The results indicate that simple growth models, first derived for colloidal synthesis<sup>22</sup>, can be used to facilitate our understanding of flame synthesis. Further, the results indicate the feasibility of studies of nanometre-scale aerosols of toxicological<sup>23</sup> and environmental<sup>24</sup> concern.

Inorganic, nanostructured materials can be produced by doping a flame with inorganic precursors contained in either a vapour or an aerosol<sup>1–3</sup>. Pyrolytic synthesis involves rapid growth of nanoparticles on the submillisecond timescale at high temperatures, typically 2,000 K. Flame reactors offer a flexible technique for tuned nanostructure synthesis<sup>5</sup>, as well as the only existing continuous process for large-scale production of nanoparticulate materials<sup>1–3</sup>. On a laboratory scale, particles of diameter between 1 and 200 nm can be produced at rates of 10–1,000 g h<sup>–1</sup> (ref. 3). Here we study the growth of silica nanoparticles in a flame.

We have recently found that third-generation synchrotron X-ray sources yield sufficient flux to easily probe time-resolved scattering signatures of nanoparticle growth in flames, even at volume fractions of the order of 10<sup>–6</sup>. At the European Synchrotron Radiation Facility (ESRF) in Grenoble, France (ID2 beam line), and at the Advanced Photon Source in Chicago (UNICAT), *in situ* observations of flames using small-angle X-ray scattering (SAXS) (G.B., H.K.K., D. J. Kohls, N.A., J. Ilavsky, S.E.P., manuscript in preparation) have helped to elucidate the dynamics of nanoparticle growth in flames. Topics investigated include the location and time of nucleation in

laminar flow fields of varying composition, the concentration and diffusion coefficient of precursor species, and the rate and homogeneity of nanoparticle growth.

A methane/oxygen diffusion flame (Fig. 1) was doped with an organometallic vapour, hexamethyldisiloxane (HMDSO), producing nanostructured silica. The apparatus was installed at the ID2 beam line, ESRF. A highly collimated monochromatic X-ray beam (12.46 keV) enters from the right of the flame, and scattered and transmitted beams pass to a 10-m evacuated flight chamber partially shown at the left of Fig. 1. A diagram of the diffusion burner and a micrograph of the powder collected on a filter, typical of this type of synthesis, are given on the right of Fig. 1. The burner shown produces 17 g h<sup>–1</sup> of nanoscale silica. Figure 2 displays the azimuthally averaged SAXS patterns from this silica aerosol, plotted as normalized scattered intensity versus scattering wave vector,  $q = (4\pi/\lambda) \sin(\theta/2)$ , where  $\lambda$  is the wavelength of the incident beam and  $\theta$  is the scattering angle. In the high- $q$  region, Porod's law<sup>25–27</sup>

$$I(q) = Bq^{-4} \quad (1)$$

is observed, indicating the presence of a smooth and sharp interface for the smallest particles (Fig. 1b);  $B$  is a constant proportional to  $S/V$ , the average surface to volume ratio for the nanoparticles. The deviation from equation (1) at low  $q$  reflects the particle size using Guinier's law<sup>25–27</sup>

$$I(q) = G \exp(-q^2 R_g^2/3) \quad (2)$$

where  $R_g$  is the radius of gyration of the primary particles within the nanoscale aggregates depicted in Fig. 1, and  $G$  is a constant proportional to the number density and average squared volume of the nanoparticles. Through the Porod invariant obtained by integrating these curves, and  $B$  of equation (1), the average surface to volume ratio can be determined<sup>25–27</sup>. The average spherical diameter is then given by  $d_p \approx 6 V/S$ . Additionally, the dimensionless ratio<sup>28</sup>

$$PDI = BR_g^4/(1.62G) \quad (3)$$

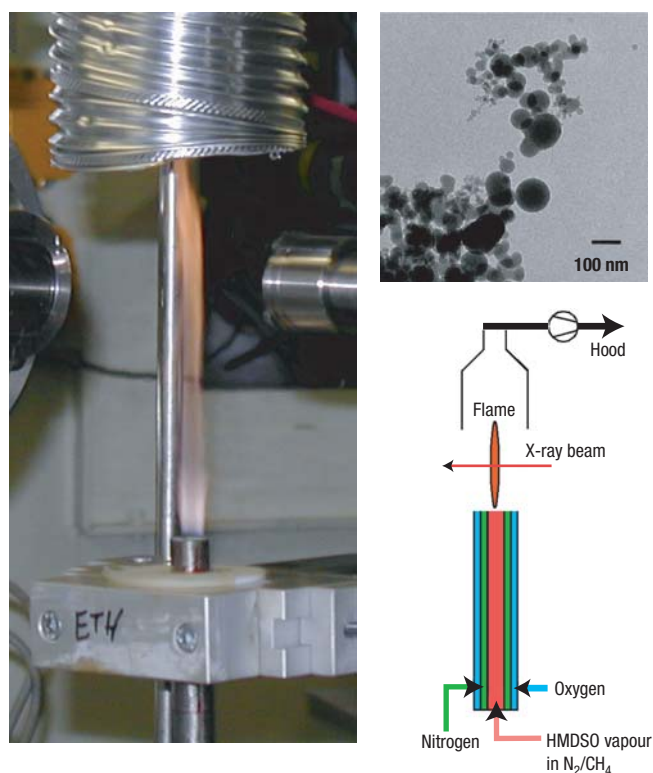


**Figure 1** Experimental set-up. Left, diffusion flame installed at the ID2 beam line, ESRF. The X-ray beam ( $\lambda \approx 0.1$  nm) is incident from the horizontal beam pipe (right side), and traverses through the flame. To the left is a 10-m evacuated chamber (not shown) housing the SAXS detector (an image intensified CCD). Right, sketch of the diffusion flame, and transmission electron micrograph of corresponding silica nanoparticles collected on a filter. HMDSO, hexamethyldisiloxane.

is a measure of the polydispersity of the particles, with 1 indicating monodisperse spheres and 5.5 reflecting the terminal dispersion expected from fully sintered spheres<sup>1,28</sup>. For spherical particles with a log-normal distribution, the geometric standard deviation is given by<sup>28</sup>  $\ln(\sigma_g) = (\ln(\text{PDI})/12)^{1/2}$ . The initial curve at 5 mm is more disperse,  $\text{PDI} = 9.1$ , than the terminal dispersion, as expected for nanoparticles undergoing nucleation with varying precursor concentration. These early particles are approximately 20 nm in diameter for this relatively hot diffusion flame ( $\sim 2,200$  K). Particles from 1 nm to  $>100$  nm can be produced, largely depending on the flame temperature and the residence time of the particles at high temperature. In this diffusion flame, particle growth is governed by mass transport, and we expect the particle size to scale with the square root of residence time<sup>22</sup>.

Through computer-controlled motion of the burner, a series of scattering patterns were collected (0.3 s per exposure) as a function of height above the burner and lateral position relative to the burner axis, as shown for axial measurements in Fig. 2. A mapping of nanoparticle growth in the flame can be produced by least-squares fitting of the data to a global scattering function based on polydisperse, smooth-surfaced, spherical particles<sup>29–32</sup>, as illustrated by the lower curve in Fig. 2. Such a mapping of silica concentration and the number density of primary particles is depicted in Fig. 3. For this diffusion flame, silica is produced throughout the flame, as oxygen must diffuse to the fuel and precursor at the centre of the flame. The conversion from

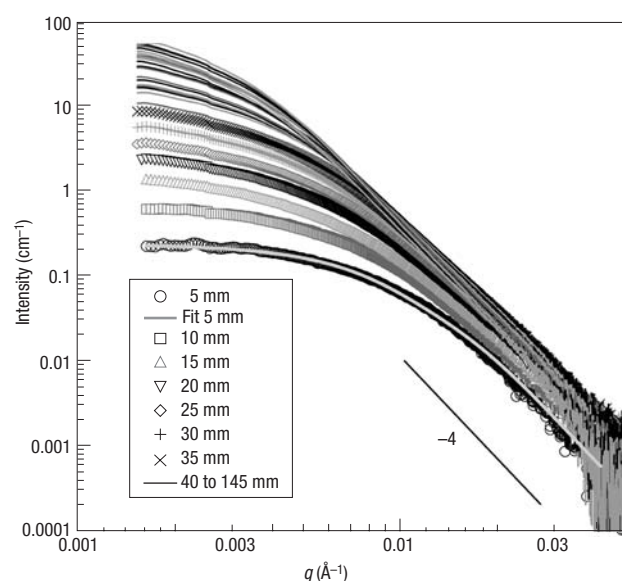


**Figure 2** Corrected, axial, scattering curves as a function of height above the burner. The solid line in the bottom data set corresponds to the fit to the unified function<sup>29–31</sup> ( $d_p = 20$  nm,  $\text{PDI} = 9.1$ ). Data monotonically increase in intensity, at lowest  $q$ , in 5-mm steps above the burner. The line labelled  $-4$  follows equation (1).

precursor to oxide appears along a conversion front that can be seen best at 10–30 mm above the burner in Fig. 3a and b as an axially symmetric region of high silica volume fraction and nanoparticle number density. The initial silica concentration at 5 mm above the burner is sufficient to rapidly produce nanoparticle nuclei (Fig. 3b) where a burst in particle number density is seen early in the flame. A height of 5 mm corresponds to the first 300  $\mu\text{s}$  of nanoparticle growth in this continuous process. The average flame temperature at this position (see Fig. 4) is approximately 2,300 K. This condition is more than sufficient for silica nanoparticles to rapidly coalesce<sup>9</sup> ( $< 1$  ms) to a low number density population of growing particles at 10 mm above the burner. Diffusion fronts at the side of the burner axis, as seen in Fig. 3 at 10 to 50 mm above the burner, allow for continued nucleation and coalescence at higher positions in the flame governed by the radial diffusion of nascent silica species to the growing nanoparticles, for instance, along the burner axis in Fig. 4b. The two-dimensional (2D) profiles in Figs 3 and 5 are slightly skewed to the left owing to a slight asymmetry in the exhaust, also seen in Fig. 1.

Figure 5 shows 2D mappings of the size and polydispersity profiles for the particles. Upon nucleation, 5 mm above the burner, relatively small (20 nm) particles of high polydispersity are formed owing to the variable conditions of nucleation and the length of time over which homogeneous nucleation occurs. This dispersion decays in width as surface growth and coalescence proceed with time in the flame. Opposing this reduction in polydispersity by coagulation is the continuous generation of silica by conversion at the diffusion front (Fig. 3a). The least polydisperse particles are seen where the largest nanoparticles occur (Fig. 5a). In these regions of high flame temperature, the particle population approaches the self-preserving limit where the PDI (and standard deviation of the particle size distribution) reaches a constant value of  $\text{PDI} = 5.5$  (refs 1, 28), corresponding to  $\sigma_g = 1.45$ , which is the self-preserving value for spheres in the free-molecular regime<sup>1</sup>. Further downstream in the flame, a fairly uniform population of nanoparticles is produced (Fig. 5b).

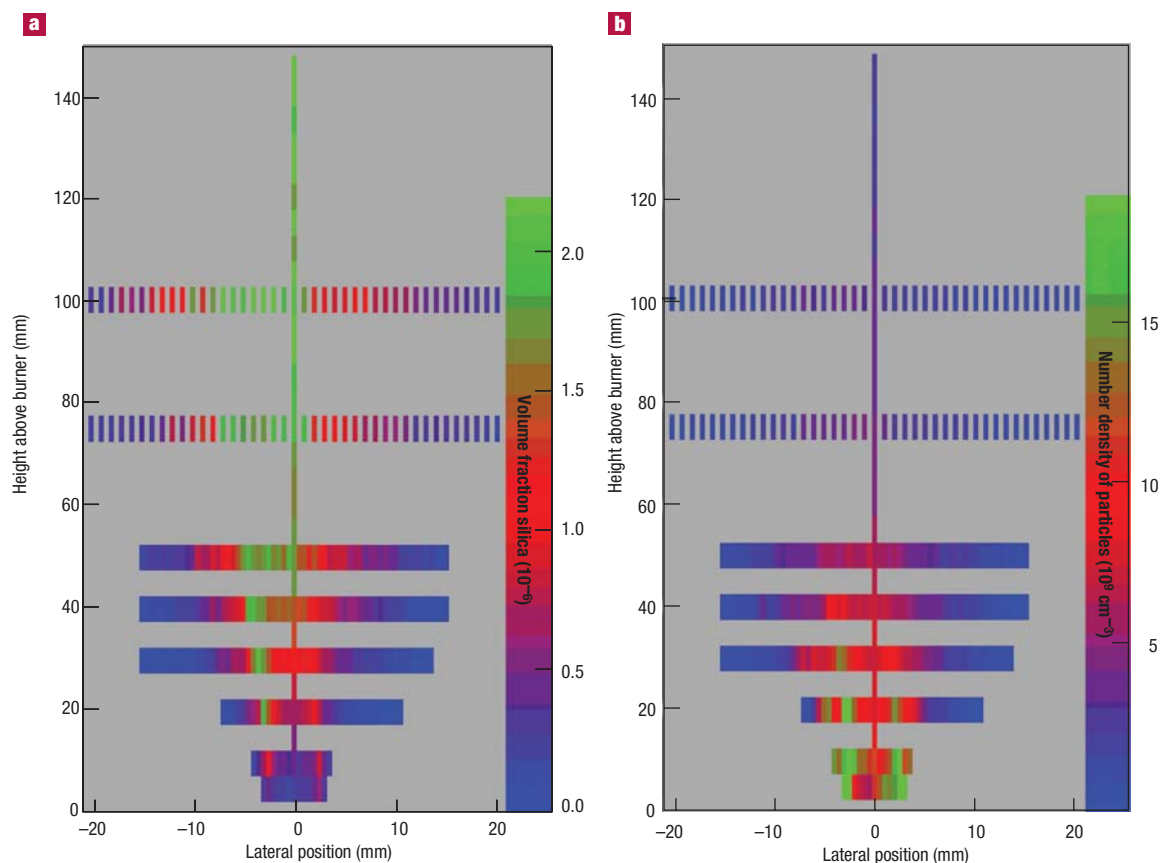


**Figure 3** 2D plots of concentration. **a**, Silica volume fraction in the diffusion flame shown in Figs 1 and 2 from global fits to scattering data and the scattering invariant<sup>25–32</sup>. **b**, Primary particle number density from the scattering invariant<sup>25–32</sup> and the Guinier prefactor,  $G$ , using a silica density of  $2.2 \text{ g cm}^{-3}$  (though slightly lower values are expected for nanoscale silica).

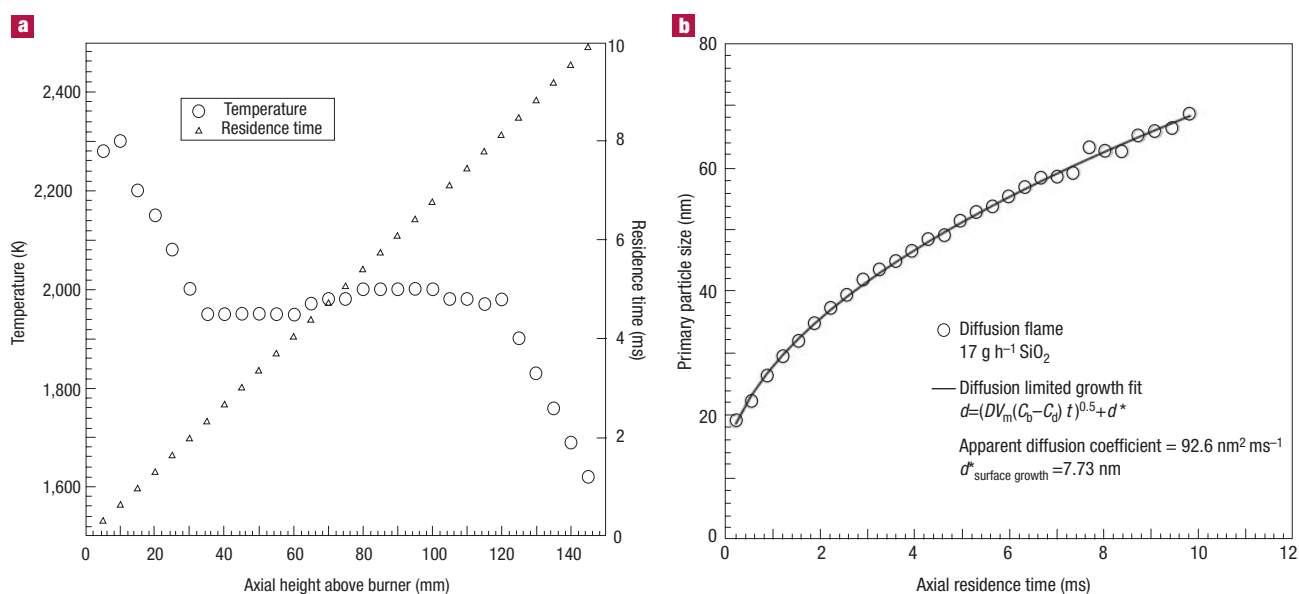


**Figure 4** Axial properties of flame. **a**, Temperature (from measurements on an identical flame) as a function of height above burner<sup>10,11</sup>. Also shown is residence time versus horizontal position (right axis). **b**, Primary particle growth rate using temperature profile for axial positions from 5 to 150 mm above the burner (Fig. 2). Fit corresponds to classical diffusion-limited surface nucleation and growth<sup>22</sup>. The apparent diffusion coefficient,  $D$ , is used to calculate  $D = 9.26 \times 10^{-5} \text{ m}^2 \text{ s}^{-1}$  at 1,900 K using a volume fraction silica of  $1 \times 10^{-6}$ , approximated from Fig. 3a. The homogeneous critical nucleus size is given by  $d^*_{\text{bulk}} = 2d^*_{\text{surface}} = 15.5 \text{ nm}$  from the fit parameter  $d^*_{\text{surface growth}}$  (ref. 22).

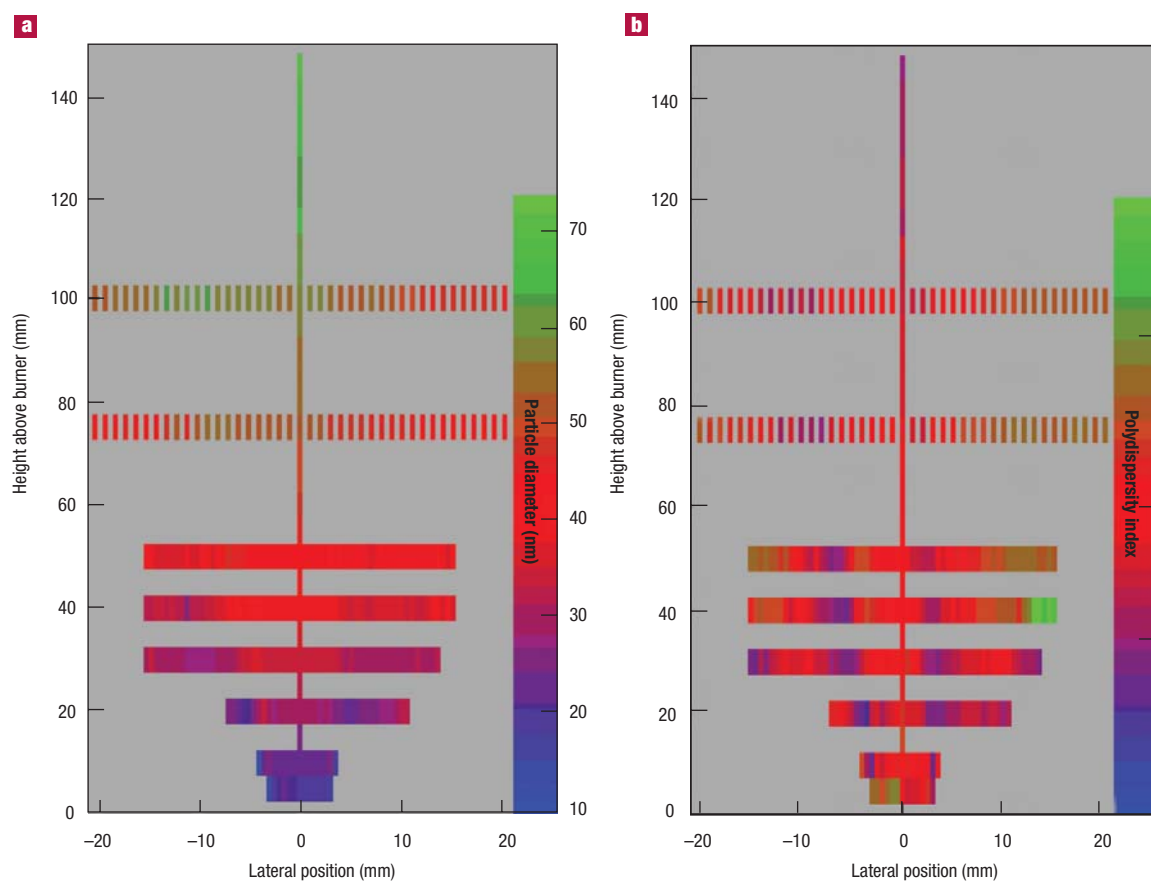


Figure 5 2D plots of nanoparticle growth. **a**, Primary particle size<sup>28,32</sup>,  $d_p$ . **b**, Primary particle polydispersity index: 1 = monodisperse, 5.5 = self-preserving limit<sup>1,28</sup>.

Powders collected from this flame were examined by nitrogen gas adsorption, transmission electron microscopy (Fig. 1) as well as by SAXS, in separate measurements, and yielded comparable size and polydispersity index:  $d_{p,BET} = 55$  nm;  $d_{p,SAXS} = 56.2$  nm and  $PDI = 8$  ( $\sigma_g = 1.52$ ).

The average temperature profile<sup>10,11</sup> of the flame depicted in Fig. 4a was determined by independent measurements using infrared spectroscopy. This temperature profile is used, together with the ideal gas law, to calculate the axial velocity of the laminar gas stream, which is of the order of  $15 \text{ m s}^{-1}$ , assuming an initial flame diameter of 6 mm and uniform and instantaneous volumetric thermal expansion. The calculated velocities are used to convert the height above the burner to residence time in the flame in Fig. 4b, which shows primary nanoparticle size as a function of time. For diffusion-limited surface growth, particle size ( $d$ ) is expected to scale with the square root of time<sup>22</sup>,

$$d = [DV_m(C_b - C_d)t]^{1/2} + d^* \quad (4)$$

where  $D$  is the diffusion coefficient for silica species that are nucleated in surface patches on growing nanoparticles,  $V_m$  is the molar volume of silica species,  $C_b$  is the bulk concentration and  $C_d$  is the concentration at equilibrium with particles of size  $d$ ,  $t$  is the time of surface growth and  $d^*$  is the minimum size for a stable surface nucleus (patch) at  $C_b$  assuming the diffusion path is much larger than the particle size and that silica species follow free molecular transport<sup>1</sup>. The critical nucleus size at

equilibrium with  $C_b$  is  $2d^*$  (ref. 22). The fit in Fig. 4b yields an apparent diffusion coefficient of  $9.26 \times 10^{-11} \text{ m}^2 \text{ s}^{-1}$  and, assuming diffusion of silica species at  $1 \times 10^{-6}$  volume fraction, the diffusion coefficient is  $9.26 \times 10^{-5} \text{ m}^2 \text{ s}^{-1}$  at about 1,900 K. The critical bulk nucleus size is about 15.5 nm, consistent with the particle size data in Fig. 4b and with sizes reported for solution synthesis<sup>33</sup>.

We have demonstrated the feasibility of *in situ* SAXS studies of the dynamics of nanoparticle growth in flames with submillisecond resolution. Direct 2D mapping of nanoparticle nucleation and growth can be made on size scales from 0.5 to 500 nm, and on timescales as short as 100  $\mu\text{s}$ , depending on the gas flow rates. The results support simple diffusion-controlled growth laws that model the data and encourage current attempts at simulation and modelling of nanoparticle growth, while offering a technique for direct verification of these predictions. Control of nanometre-scale structure for many applications requires such understanding of the basic physical principles involved in their formation.

## METHODS

Figure 1 shows a schematic drawing of the diffusion burner that is fed with three streams of gas/vapour through temperature-controlled lines using mass flow controllers: the central burner tube carries methane (at  $1.45 \text{ l min}^{-1}$  STP) and nitrogen (at  $2.9 \text{ l min}^{-1}$  STP), used as a carrier gas, fed through a flask of hexamethyldisiloxane (HMDSO),  $5^\circ\text{C}$ . This results in  $0.28 \text{ g min}^{-1}$  of HMDSO being fed by the carrier gas with a calculated production rate of  $17 \text{ g h}^{-1} \text{ SiO}_2$ . The second annulus carries a diluent nitrogen stream at  $0.5 \text{ l min}^{-1}$  STP. An oxygen stream is fed to the outer annulus at  $8 \text{ l min}^{-1}$ . At 2,200 K and using an initial flame diameter of 6 mm, these flow rates correspond to about  $66 \mu\text{s}$  per mm height above the burner.

The lowest height above the burner that can routinely be measured is 0.4 mm (26  $\mu$ s), and steps of 0.2 mm (13  $\mu$ s) are used low in the flame. The first point shown in Fig. 5b is at 5 mm (0.3 ms), reflecting the time resolution needed for diffusion-limited surface growth. The flame is typical for pyrolytic synthesis in a laminar, diffusion flame.

The X-ray beam was 300  $\mu$ m in diameter and the exposure time was 0.3 s, although exposures as short as 10 ms are possible with this instrument. Data are corrected by a procedure reported elsewhere<sup>33</sup>, including subtraction of background measurements made on similar flames in the absence of the silica precursor. The absolute intensity (Fig. 2) is obtained using a flame diameter of 6 mm.

The scattering data are evaluated using the unified function<sup>28–31</sup>, which combines local scattering laws, specifically equations (1) and (2), in a global equation as described elsewhere<sup>29,30</sup>. Mass fractal dimension and aggregate/agglomerate size can also be measured using SAXS, and will be reported elsewhere (G.B., H.K.K., D.J. Kohls, N.A., J. Ilavsky and S.E.P., manuscript in preparation).

Received 5 January 2004; accepted 2 April 2004; published 16 May 2004.

## References

- Friedlander, S. K. *Smoke, Dust, and Haze: Fundamentals of Aerosol Dynamics* 2nd edn (Oxford Univ. Press, New York, 2000).
- Ulrich, G. D. Flame synthesis of fine particles. *Chem. Eng. News* **62**, 22–29 (1984).
- Pratsinis, S. E. Flame aerosol synthesis of ceramic powders. *Prog. Energy Combust. Sci.* **24**, 197–219 (1998).
- Van der Wal, R. L., Berger, G. M. & Hall, L. J. Single-walled carbon nanotube synthesis via a multi-stage flame configuration. *J. Phys. Chem. B* **106**, 3564–3567 (2002).
- Madler, L., Stark, W. J. & Pratsinis, S. E. Rapid synthesis of stable ZnO quantum dots. *J. Appl. Phys.* **92**, 6537–6540 (2002).
- Stark, W. J., Pratsinis, S. E. & Baiker, A. Flame made titania/silica epoxidation catalysts. *J. Catal.* **203**, 516–524 (2001).
- Madler, L., Stark, W. J. & Pratsinis, S. E. Flame-made ceria nanoparticles. *J. Mater. Res.* **17**, 1356–1362 (2002).
- Anala, S. *et al.* In situ NMR spectroscopy of combustion. *J. Am. Chem. Soc.* **125**, 13298–13302 (2003).
- Tsantilis, S., Briesen, H. & Pratsinis, S. E. Sintering time for silica particle growth. *Aerosol Sci. Technol.* **34**, 237–246 (2001).
- Arabi-Katbi, O. I., Pratsinis, S. E., Morrison, P. W. Jr & Megaridis, C. M. Monitoring the flame synthesis of TiO<sub>2</sub> particles by in-situ FTIR spectroscopy and thermophoretic sampling. *Combust. Flame* **124**, 560–572 (2001).
- Morrison, P. W., Raghavan, R., Timpone, A. J., Artelt, C. P. & Pratsinis, S. E. In situ Fourier transform infrared characterization of the effect of electrical fields on the flame synthesis of TiO<sub>2</sub> particles. *Chem. Mater.* **9**, 2702–2708 (1997).
- Dobbins, R. A. & Megaridis, C. M. Morphology of flame-generated soot as determined by thermophoretic sampling. *Langmuir* **3**, 254–259 (1987).
- Köylü, Ü. Ö., McEnally, C. S., Rosner, D. E. & Pfefferle, L. D. Simultaneous measurements of soot volume fraction and particle size / microstructure in flames using a thermophoretic sampling technique. *Combust. Flame* **110**, 494–507 (1997).
- Hurd, A. J. & Flower, W. L. In situ growth and structure of fractal silica aggregates in a flame. *J. Colloid Interface Sci.* **122**, 178–192 (1988).
- Xing, Y., Köylü, Ü. Ö. & Rosner, D. E. In situ light-scattering measurements of morphologically evolving flame-synthesized oxide nanoaggregates. *Appl. Opt.* **38**, 2686–2697 (1999).
- King, G. B., Sorensen, C. M., Lester, T. W. & Merklin, J. F. Direct measurements of aerosol diffusion constants in the intermediate Knudsen regime. *Phys. Rev. Lett.* **50**, 1125–1128 (1983).
- Chowdhury, D. P., Sorensen, C. M., Taylor, T. W., Merklin, J. F. & Lester, T. W. Application of photon correlation spectroscopy to flowing brownian motion systems. *Appl. Opt.* **23**, 4149–4154 (1984).
- Taylor, T. W. & Sorensen, C. M. Gaussian beam effects on the photon correlation spectrum from a flowing brownian motion system. *Appl. Opt.* **25**, 2421–2426 (1986).
- Sorensen, C. M., Hageman, W. B., Rush, T. J., Huang, H. & Oh, C. Aerogelation in a flame soot aerosol. *Phys. Rev. Lett.* **80**, 1782–1785 (1998).
- Sorensen, C. M., Hagemann, W. B. Two-dimensional soot. *Langmuir* **17**, 5431–5434 (2001).
- Zachariah, M. R. & Semerjian, H. G. Simulation of ceramic particle formation: Comparison with in-situ measurements. *Am. Inst. Chem. Eng. J.* **35**, 2003–2012 (1989).
- Sugimoto, T. *Monodisperse Particles* (Elsevier, New York, 2001).
- Pyne, S. Small particles add up to big disease risk. *Science* **295**, 1994 (2002).
- Chameides, W. L. & Bergin, M. Soot takes center stage. *Science* **297**, 2214–2215 (2002).
- Guinier, A. & Fournet, G. *Small Angle Scattering of X-rays* (John Wiley & Sons, New York, 1955).
- Glatter, O. & Kratky, O. *Small-angle X-ray Scattering* (Academic, London, 1982).
- Roe, R.-J. *Methods of X-Ray and Neutron Scattering in Polymer Science* (Oxford Univ. Press, New York, 2000).
- Beaucage, G., Kammler, H. K. & Pratsinis, S. E. Estimate of particle-size polydispersity from small-angle scattering. *J. Appl. Crystallogr.* (in the press).
- Beaucage, G. Approximations leading to a unified exponential/power-law approach to small-angle scattering. *J. Appl. Crystallogr.* **28**, 717–728 (1995).
- Beaucage, G. Small-angle scattering from polymeric mass fractals of arbitrary mass-fractal dimension. *J. Appl. Crystallogr.* **29**, 134–146 (1996).
- Hyeon-Lee, J., Beaucage, G., Pratsinis, S. E. & Vemury, S. Fractal analysis of flame-synthesized nanostructured silica and titania powders using small-angle X-ray scattering. *Langmuir* **14**, 5751–5756 (1998).
- Kammler, H. K., Beaucage, G., Mueller, R. & Pratsinis, S. E. Structure of flame-made silica nanoparticles by ultra small-angle x-ray scattering. *Langmuir* **20**, 1915–1921 (2004).
- Pontoni, D., Narayanan, T. & Rennie, A. R. Time-resolved SAXS study of nucleation and growth of silica colloids. *Langmuir* **18**, 56–59 (2002).

## Acknowledgements

This work was supported by the US National Science Foundation (CTS-0070214), the Swiss National Science Foundation (200021-101901/1), the Swiss Commission for Technology and Innovation (TopNano21-5487.1) and the synchrotron facilities at ESRF (beam time allocation ME421). We thank J. Gorini for technical assistance; we also thank D. J. Kohls (at the University of Cincinnati), and J. Ilavsky and P. Jemian (at UNICAT, Advanced Photon Source) for collaborative work. G.B. thanks the University of Cincinnati for sabbatical leave at ETH Zentrum.

Correspondence and requests for materials should be addressed to G.B.

## Competing financial interests

The authors declare that they have no competing financial interests.